

Article

In Vitro Assessment of Sericin-Silver Functionalized Silk Fabrics for Enhanced UV Protection and Antibacterial Properties Using Experimental Design

Pisutsaran Chitichotpanya ^{1,*} and Chayanisa Chitichotpanya ^{2,3}

¹ Department of Materials and Textile Technology, Faculty of Science and Technology, Thammasat University, Pathumthani 12121, Thailand

² Department of Chemistry, Faculty of Science, Mahidol University, Bangkok 10400, Thailand; chayanisa.chi@mahidol.ac.th

³ Center for Surface Science and Engineering, Faculty of Science, Mahidol University, Bangkok 10400, Thailand

* Correspondence: pisut_c@tu.ac.th or pisutsaran@gmail.com; Tel.: +66-9297-989-65

Received: 22 July 2017; Accepted: 8 September 2017; Published: 13 September 2017

Abstract: Silk sericin (SS) was used as both a 3-dimensional matrix and reductant for the in situ synthesis of silver nanoparticles (AgNPs) finished on silk fabrics. We demonstrated enhanced UV protection and antibacterial properties using this synthesis which was an environmental friendly approach. Development and optimization was achieved using a central composite design (CCD) in conjunction with the response surface methodology (RSM). The goal was to identify the concentrations of SS and AgNO₃ that produced the optimal balance between UV protection and antibacterial activity, when tested against *E. coli* and *S. aureus*. The SS-AgNP bio-nanocomposites were characterized using Scanning Electron Microscope (SEM-EDX), X-ray diffraction (XRD), X-ray photoelectron spectroscopy (XPS), and Fourier transform infrared spectroscopy (FTIR). Statistical analyses indicated an empirical second-order polynomial could accurately model the experimental values. To confirm that the optimal levels from RSM worked in practice, performance evaluations were conducted, including tests of cytotoxicity, of the durability and stability of UV protection, as well as of the antibacterial activity of the functionalized fabrics after repeated standard washing. The results suggest that these bio-nanocomposites have great potential for multi-functionalization on silk fabrics. Our method has been shown to convert the waste material (SS) to a fabric with high added value.

Keywords: sericin; silver nanoparticles; response surface methodology; antibacterial activity; silk fabric

1. Introduction

Recently, ultraviolet (UV) protection finishing of fibers or fabrics has received much attention. Long-term exposure to UV light can lead to a series of negative health effects; for instance, acceleration of skin ageing, photodermatosis (acne), erythema (skin reddening), and even severe skin cancer [1]. Other than drastically avoiding exposure to sun light, the most frequently recommended form of UV protection is the use of sunscreens, hats, and proper selection of clothing. Clothing fabrics are good protectors against UV radiation. However, the level of protection offered depends on many different factors such as fiber composition, fabric construction, and wet-processing of the fabrics such as color and other finishing treatments applied to the textile material [2]. Different types of UV protective finishes have been developed, giving excellent UV protection to textiles. Titanium dioxide and zinc oxide nanoparticles (NPs) have been widely used, as they provide protection by reflecting, scattering, or absorbing harmful UV [3–5]. UV protection has also been imparted to fabrics using dyes

obtained from natural sources [6,7]. The use of biopolymer finishing agents is a field with potentially great benefits.

Sericin (SS) is a natural macromolecular protein, mainly amorphous and glue-like, which serves as a gum adhesive to sustain the structural strength of the silk cocoon [8]. The silk fiber comprises a protein fibroin surrounded with SS. SS has been regarded as a waste product and generally discarded in the manufacture of silk fibroin. Most of it is removed during the degumming process of cocoon silk. SS exhibits several biological activities and has proven to be biocompatible. It consists of 18 amino acids, and the combination of serine-rich sequences with aspartic acid is responsible for its hydrophilicity. It is sensitive to chemical modification because of its strong polar side chains: hydroxyl, carboxyl, and amino groups [9]. SS has been extensively studied for many potential applications because of its unique biochemical and biophysical properties including biocompatibility, biodegradability, UV protection, as well as antibacterial and antioxidant activities [10,11]. SS offers UVB protection by reducing oxidative stress on the skin [12]. It has been reported that approximately 50,000 tons of SS could be recovered from the waste solution out of one million tons of fresh cocoon [13,14]. This discarded SS solution can cause environmental contamination due to its high oxygen demand when degraded by microorganisms [15]. Adding value to SS waste could therefore have significant economic and social benefits.

Development of multifunctional finishing of textile materials has received great interest. Bio-nanocomposites are a new generation of nanocomposite materials. They comprise a natural polymer matrix and organic/inorganic nano-fillers [16]. These bio-nanocomposites are biodegradable and biocompatible, and can be used in various medical, agricultural, drug release, and packaging applications [17]. In terms of antibacterial activity, silver nanoparticles (AgNPs) have received the most attention because of their broad antibacterial spectrum against yeasts, fungi, viruses, and bacteria, and their established use in the medical field. The stability and distribution of AgNPs are significant in antibacterial and mechanical properties. SS is a promising polymer matrix for such materials, as it is capable of metal ion chelating capability and can form chemical bonds with transition metals, enhancing the stability of the NPs. In addition, since it has redox activities [18–20], it can induce the reduction of Ag^+ to AgNPs [21,22].

Since silk textile is one of the most important industries in Thailand, efforts to add value to silk fibers have focused on enhancing end-use performance. This paper presents a simple, economical, non-toxic, and environmental friendly process for imparting UV and antibacterial properties to silk fabrics. This involved the in situ synthesis of AgNPs using SS as a reducing agent, stabilizer, and binder. The goal was to identify the concentrations of SS and AgNO_3 that produced the optimal balance between UV protection and antibacterial activity against two strains of bacteria: *Escherichia coli* (*E. coli*) and *Staphylococcus aureus* (*S. aureus*), using response surface methodology (RSM). To confirm that these optimal levels from RSM worked in practice, performance evaluations were conducted, including tests of cytotoxicity, of the durability and stability of UV protection, and of the antibacterial activity of the functionalized fabrics after repeated standard washing.

2. Experimental

2.1. Materials and Chemicals

Silk fabrics, and fresh cocoons from *Bombyxmori* silkworms produced in a controlled environment, were donated by Chul Thai Silk Farm, Petchaboon, Thailand. Silver nitrate (AgNO_3) was purchased from Sigma-Aldrich (Bangkok, Thailand). All chemicals were of analytical grade. *S. aureus* (ATCC 6538) and *E. coli* (ATCC 8739) were used for determining the antimicrobial activity.

2.2. Preparation of SS Solution

SS was isolated from the cocoon by degumming under high temperature and pressure [21]. Briefly, the silk cocoons were soaked in deionized (DI) water at a ratio of dry silk cocoon: DI water of 1 g:30 mL.

The mixture was degummed using an autoclave at 100 °C for 60 min. Fibroin fibers were isolated by filtration, and the remaining SS solution was concentrated to 7 wt %, determined by a bicinchoninic acid (BCA) protein assay (Pierce, Rockford, IL, USA). This SS solution was used as a stock solution. The molecular weights of the obtained SS were in the range of 25–150 kDa, as reported previously [23].

2.3. Functionalization of Silk Fabrics by SS-AgNP Bio-Nanocomposites

Scoured silk fabric pieces (20 cm × 20 cm, 2.4 g in weight) were immersed in the SS solution that was diluted to the desired concentration and the pH adjusted to 11 by NaOH [21]. Aqueous solutions of AgNO₃ were prepared by dissolving AgNO₃ in DI water. The AgNO₃ solution was added to the SS solution under stirring for 24 h at room temperature to complete the conversion of Ag⁺ to Ag⁰ nanoparticles.

2.4. Experimental Design and Data Analysis

The SS-AgNP nanocomposites were prepared using RSM. It is an effective and practical tool to optimize preparation conditions within a multivariable system as a classical one-variable-at-a-time methodology cannot be used to study the combined effects of two or more variables on a measured response [24]. It is used to evaluate the interactions of various variables simultaneously and provide an empirical description of the effects of variables and their interactions on a measured response. Two independent variables (contents of SS (X_1) and AgNO₃ (X_2)) were evaluated using the central composite design (CCD) in conjunction with RSM to determine the optimal conditions. Preliminary trials were conducted to identify the range of each input variable and the minimum number of experimental runs. To determine the best SS concentration that achieved the most uniform coating, three samples were prepared: 7500 ppm, 10,000 ppm, and 12,500 ppm, based on the work reported by Lu et al. [20]. Three samples with different AgNO₃ contents were prepared: 750 ppm, 1000 ppm, and 1500 ppm. In a preliminary test, the antibacterial activities against *E. coli* strain of these samples exhibited 76%, 92%, and 100% reductions of colony forming units (CFU), respectively. Therefore, the AgNO₃ levels in the main experiments were set in the range of 890 to 1605 ppm. The independent variables were the SS (X_1 , ppm) and AgNO₃ (X_2 , ppm) contents at five levels, as shown in Table 1. The ultraviolet protection factor (UPF) (Y_1), %reduction of *E. coli* (Y_2 , %), and %reduction of *S. aureus* (Y_3 , %) were selected as the dependent variables. The design matrix, including the dependent and independent variables, is presented in Table 2. The interaction of independent variables and measured responses were modeled using the following quadratic mathematical model (see Equation (1)):

$$Y = b_0 + b_1X_1 + b_2X_2 + b_{12}X_1X_2 + b_{11}X_1^2 + b_{22}X_2^2 \quad (1)$$

where Y is the predicted response, b_0 is the intercept, and b_1 and b_2 are the regression coefficients. X_1 and X_2 are individual effects, X_1X_2 is the interaction effect, and X_1^2 and X_2^2 are the quadratic effects. An analysis of variance (ANOVA) was conducted to determine the statistical significance of the model at a confidence level of 95% ($p < 0.05$).

Table 1. Experimental range and coded levels of independent variable ($\alpha = 1.414$).

Variable	Symbol	Coded Levels				
		$-\alpha$	-1	0	1	α
AgNO ₃ (ppm)	X_1	896.5	1000	1250	1500	1603.5
Silk sericin (SS) (ppm)	X_2	6465	7500	10,000	12,500	13,535

2.5. Characterization of SS-AgNP Bio-Nanocomposites

The SS-AgNP bio-nanocomposites were characterized by X-ray photoelectron spectroscopy (XPS, Axis Ultra DLD, Kratos Analytical Ltd., Manchester, UK), Fourier transform infrared spectroscopy

(FTIR, Niclolet 6700 FT-IR spectrometer/Thermo, Fisher Scientific, Hampton, NH, USA), and X-ray diffraction (XRD, D8 Advance, Bruker Corporation, Karlsruhe, Germany). The X-ray diffraction (XRD) measurements were performed over the 2θ range of $20\text{--}80^\circ$ at a scan speed of $6^\circ \text{C min}^{-1}$, using a Cu anode ($\lambda = 0.154 \text{ nm}$) at 40 kV and 40 mA. The morphology of the nanocomposites was investigated by Field Emission Scanning Electron Microscopy, equipped with Energy-dispersive X-ray spectroscopy (FE-SEM, Model JSM 7610F, JEOL Inc., Peabody, MA, USA). The FE-SEM samples were coated with thin gold film by sputtering, prior to observation. The size of AgNPs were determined by Zetasizer 3000HS (Malvern Instruments, Worcestershire, UK). The measurement was performed using a He-Ne laser beam of 633 nm wavelength with a fixed scattering angle of 90° at 25°C .

2.6. Color Measurement

Color values of treated samples were calculated from the diffuse reflectance measured with a spectrophotometer (Hunter Lab Color Quest XE, Reston, VA, USA). Color coordinates were determined in the CIELab color space (L^* , a^* , b^*) for the 10° standard observer and D65 standard illuminant. L^* corresponds to the brightness (0 = black, 100 = white), a^* to the red-green coordinate (−ve = green, +ve = red), and b^* to the yellow-blue coordinate (−ve = blue, +ve = yellow). The color difference is expressed as ΔE^* and can be calculated using the following Equation (2):

$$\Delta E^* = \sqrt{(\Delta L^*)^2 + (\Delta a^*)^2 + (\Delta b^*)^2} \quad (2)$$

where ΔE^* is the CIELab color difference between untreated and treated cottons.

All color measurements were repeated three times for each sample at different sample positions.

2.7. Contact Angle Measurement

The surface contact angles were measured with a water contact angle (Drop Shape Analyzer, DSA25, Hamburg, Germany). The samples were cut down to $25 \text{ mm} \times 25 \text{ mm}$. and attached to the base of the equipment. A drop of deionized water was deposited on the surface of the samples using a graduated syringe. All the contact angles were measured by a sessile drop method at five different sites on each sample. The contact angles were obtained by photographs and submitted to software analysis for 10 s.

2.8. Determination of Ultraviolet Protection Factor (AS/NZS 4399:1996)

The UV protection properties of treated fabrics were evaluated against the ultraviolet protection factor (UPF), following the AS/NZS 4399: 1996 test method [25]. The UPF rating was determined using the following Equation (3):

$$\text{UPF} = \frac{\sum_{290 \text{ nm}}^{400 \text{ nm}} E_\lambda S_\lambda \Delta\lambda}{\sum_{290 \text{ nm}}^{400 \text{ nm}} E_\lambda S_\lambda T_\lambda \Delta\lambda} \quad (3)$$

where E_λ is the relative erythemal spectral effectiveness, S_λ is the solar spectral irradiance, T_λ is the average spectral transmittance of the specimen (measured), and $\Delta\lambda$ is the measured wavelength interval (nm). Fabrics with a UPF value in the range 15 to 24 are defined in the standard as offering “good UV protection”: From 25 to 39 as offering “very good UV protection” and 40 or greater as “excellent UV protection”.

2.9. Antimicrobial Activity Test (AATCC Test Method 100-1999)

The antibacterial activity of the fabric samples was tested following the AATCC Test Method 100-1999 [26]. All samples were sterilized by 15-min UV exposure. The samples were inoculated with 1.0 mL of inoculum containing 10^5 CFU (colony forming units) of either Gram-positive *S. aureus* (ATCC 6538) or Gram-negative *E. coli* (ATCC 8739). After incubation at 37°C for 24 h, the %reduction

in colony numbers in the treated samples was compared with that of the untreated control, using the following Equation (4):

$$\% \text{reduction} = 100 \times (A - B) / A \quad (4)$$

where A and B are the number of bacteria recovered from the untreated and treated fabric swatches respectively, after inoculation and incubation.

2.10. Washing Fastness (AATCC Test Method 61-1996)

The durability and stability of UV protection and antibacterial activity of functionalized fabrics after repeated standard washing (AATCC test method 61-1996 [27]) were evaluated after washing for 10 and 20 cycles.

2.11. The Ag^+ Ion Release Profile

The Ag^+ ion releasing profile of SS-AgNP finished silk samples was investigated. The finished samples with a size of $5.0 \times 5.0 \text{ cm}^2$ were prepared. Then, the sample was soaked in 20 mL DI water, with fresh DI water of 20 mL replaced every 12 h. The Ag^+ in solutions was determined using a Graphite Furnace Atomic Absorption Spectrometer (GF-AAS, Model A Analyst 600, Perkin Elmer, Waltham, MA, USA).

2.12. Cytotoxicity Test (MTT Assay/ISO 10993 Standard [28])

The cytotoxicity of the fabric samples was tested using the MTT (3-(4, 5-dimethylthiazol-2-yl)-2, 5-diphenyltetrazolium bromide) assay. L929 cells were seeded into 96-well plates and maintained in culture for 24 h to form a semi-confluent monolayer. The culture medium of L929 cells was removed. Then, 100 μL of sample extract solution was added to the L929 cells and incubated at 37°C with 5% CO_2 for 24 h. The culture medium of the tested cells was removed. Next, 5.0 μL of MTT solution was added to the tested cells and incubated at 37°C with 5% CO_2 for 2 h. The MTT solutions were removed from the plate, and 100.0 μL of isopropanol was added to the tested cells while swaying the plate. Finally, the absorption of the tested cell solution at a wavelength of 570 nm was determined. The %cell viability of the samples was calculated as Equation (5):

$$\% \text{cell viability} = \frac{\text{OD}_{570\text{e}} \times 100}{\text{OD}_{570\text{b}}} \quad (5)$$

where $\text{OD}_{570\text{e}}$ = the mean value of the measured optical density of the 100% extract of the test sample; $\text{OD}_{570\text{b}}$ = the mean value of the measured optical density of the blank.

If %cell viability >70% of blank, the sample was assumed to be non-cytotoxic.

3. Results and Discussion

3.1. Optimization of SS-AgNP Bio-Nanocomposites by RSM

The results of the CCD experiments to investigate the effects of the two independent variables together with the predicted and actual responses are shown in Table 2. In this study, the experimental data fit well with the empirical second-order polynomial models. The application of RSM produced the following equations for UPF (Y_1), %reduction of *E. coli* (Y_2), and %reduction of *S. aureus* (Y_3) of the nanocomposite coatings.

$$Y_1 = -26.544 + 0.021X_1 + 0.007X_2 - 2.360 \times 10^{-7}X_1X_2 - 4.555 \times 10^{-6}X_1^2 - 1.976 \times 10^{-7}X_2^2 \quad (6)$$

$$Y_2 = -184.038 + 0.131X_1 + 0.042X_2 + 4 \times 10^{-7}X_1X_2 - 4.866 \times 10^{-5}X_1^2 - 2.287 \times 10^{-6}X_2^2 \quad (7)$$

$$Y_3 = -347.921 + 0.251X_1 + 0.058X_2 - 4 \times 10^{-7}X_1X_2 - 8.967 \times 10^{-5}X_1^2 - 3.057 \times 10^{-6}X_2^2 \quad (8)$$

where X_1 is the content of SS (ppm) and X_2 is the content of AgNO_3 (ppm).

To check the adequacy of the second-order models, a significance test and ANOVA were used. Comparing the data between experiments and the RSM (predicted values), the 3D scatter graphs of UPF (Y_1), %reduction of *E. coli* (Y_2), and %reduction of *S. aureus* (Y_3) were plotted (Figure 1). The estimated regression coefficients for Y_1 , Y_2 , and Y_3 of the nanocomposite coatings are shown in Figure S1 (see Supplementary Materials). The probability of the coefficients was greater than 0.05, indicating no significant effect on the predicted responses. The determination coefficient (R^2) for Y_1 was 0.970, which implied that only 3% of the variation could not be explained by this model. Y_2 and Y_3 gave R^2 of 0.969 and 0.959, respectively. The high value of R^2 suggested that the model was significant and the experimental values agreed very well with the predicted ones, providing a good predictability of the models.

To determine the optimal conditions for excellent UV protection and antibacterial activities (>99% reduction) of the nanocomposite coatings, the 3D response surface technique was employed to determine the effects of the independent variables on Y_1 , Y_2 , and Y_3 . The results are presented in Figure 2. The predicted optimal contents of SS and AgNO_3 are shown in Table 3.

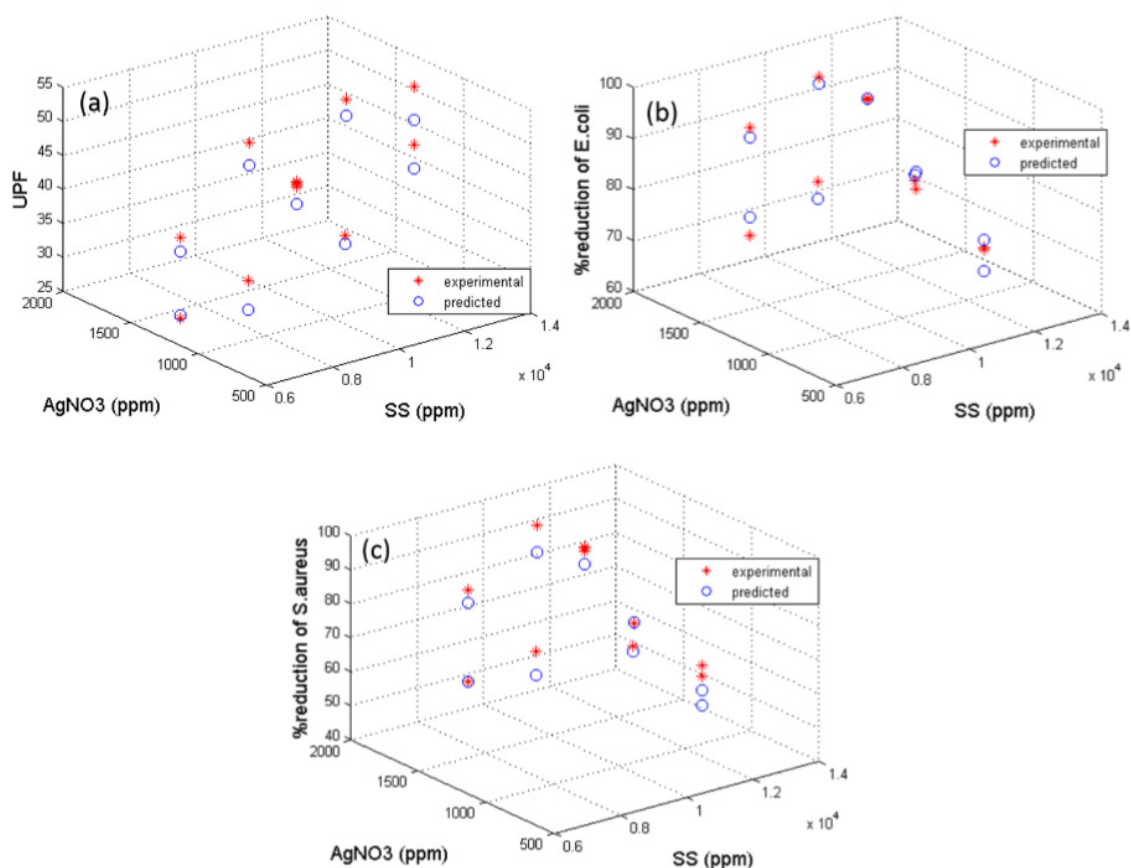


Figure 1. Predicted vs. experimental values at different levels of SS and AgNO_3 for (a) UPF (Y_1); (b) %reduction of *E. coli* (Y_2); and (c) %reduction of *S. aureus* (Y_3).

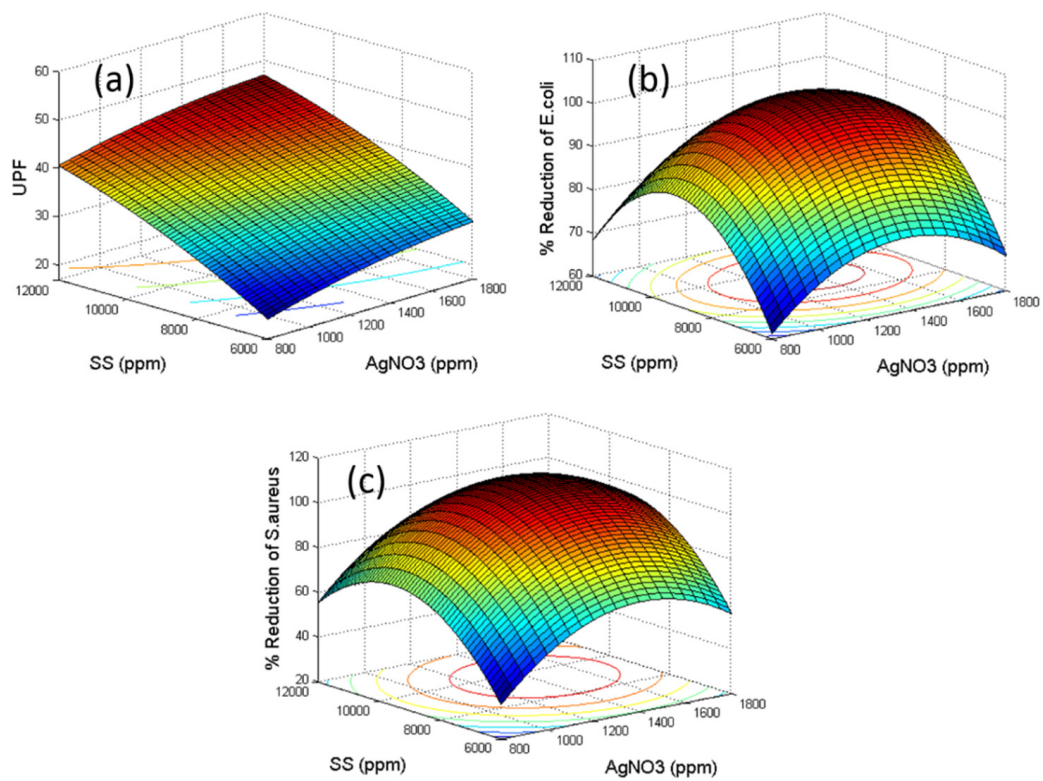


Figure 2. 3D response surface images at different levels of SS and AgNO₃ for (a) UPF, (b) %reduction of *E. coli*, and (c) %reduction of *S. aureus*.

Table 2. Experimental and predicted response surface methodology (RSM) results for Y₁, Y₂, and Y₃. X₁ and X₂ are the contents of SS (ppm) and AgNO₃ (ppm) respectively.

No.	Variable		Response Y ₁ UV Protection Factor (UPF)		Response Y ₂ (%reduction of <i>E. coli</i>)		Response Y ₃ (%reduction of <i>S. aureus</i>)	
	X ₁	X ₂	Actual	Predicted	Actual	Predicted	Actual	Predicted
1	7500	1000	33.7	29.5	91.2	87.7	80.3	73.5
2	12,500	1000	47.1	43.6	69.5	71.0	59.8	55.8
3	7500	1500	35.6	33.4	95.7	93.8	89.4	85.4
4	12,500	1500	49.3	46.9	74.7	78.1	66.4	66.7
5	10,000	896.5	38.1	36.8	88.3	89.2	77.2	75.8
6	10,000	1603.5	45.2	41.9	100.0	98.6	100.0	91.9
7	6465	1250	27.2	27.7	79.4	82.9	69.5	69.7
8	13,535	1250	52.1	47.1	64.2	60.0	55.8	43.9
9	10,000	1250	42.3	39.9	100.0	100.0	99.8	95.0
10	10,000	1250	42.0	39.9	99.8	100.0	100.0	95.0
11	10,000	1250	42.6	39.9	100.0	100.0	98.7	95.0
12	10,000	1250	42.7	39.9	100.0	100.0	100.0	95.0
13	10,000	1250	42.3	39.9	100.0	100.0	100.0	95.0
14	10,000	1250	42.8	39.9	100.0	100.0	99.6	95.0

Table 3. Optimum condition for the properties of UPF and antibacterial activity against *E. coli* and *S. aureus* of the SS-AgNP sample.

SS Content (ppm)	AgNO ₃ Content (ppm)	Size (nm)	UPF	%reduction of <i>E. coli</i>	%reduction of <i>S. aureus</i>
9800	1300	39.4 ± 8.6	40.0	100.0	97.9

3.2. Characterization of SS-AgNP and Functionalized Silk Fabrics

In this study, the Ag nanocomposites were prepared via the in situ biosynthesis using SS as a reducing and capping agent. The schematic mechanism of the AgNP reduction in SS matrix is presented in Figure 3. The Ag ions first complexed with the SS, and then were reduced to NPs. The AgNPs were surrounded by the amide, hydroxyl, and carboxyl groups of the SS, which served as a capping agent. These functional groups are able to attract silver ions and provide an electron source for the Ag reduction process. The major role of the SS was to prevent aggregation of nuclei of the NPs by inducing repulsive forces to overcome the van der Waals forces between the crystals of the individual atoms. This provided stability and uniform distribution of AgNPs in SS matrix.

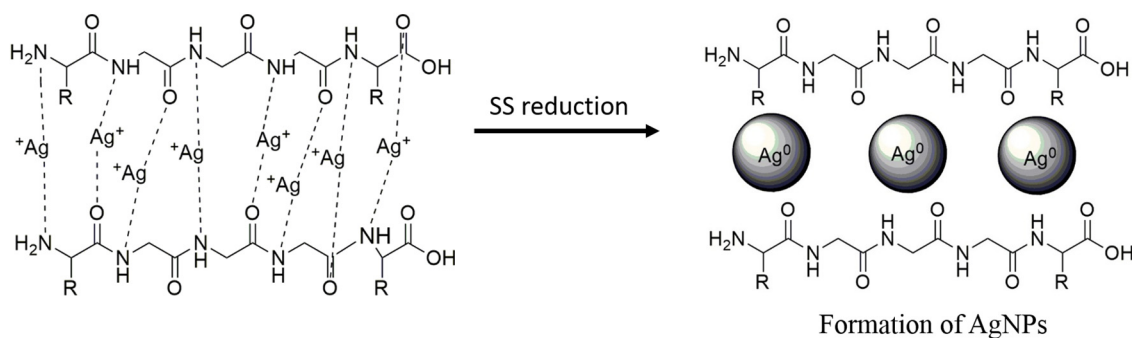


Figure 3. Schematic mechanism of the in situ synthesis of SS-Ag nanocomposite.

All FTIR spectra showed three characteristic peaks of Amide III ($1300\text{--}1200\text{ cm}^{-1}$), II ($1560\text{--}1500\text{ cm}^{-1}$), and I ($1700\text{--}1600\text{ cm}^{-1}$) of silk fiber at 1219 , 1507 , and 1614 cm^{-1} respectively [21]. After functionalization with SS-AgNP, the band position of the silk fiber shifted (Figure 4). For example, the band position at 3264 cm^{-1} , corresponding to amide A (NH stretching vibration modes), shifted to a higher region (3277 cm^{-1}) due to the formation of AgNPs. The band positions of Amide III, II, and I at 1219 , 1507 , and 1614 cm^{-1} moved to higher regions of 1226 , 1512 , and 1619 cm^{-1} , respectively. This suggested that there were interactions between silk fibers and SS-AgNP [21,29]. This might be explained by the fact that SS-AgNP nanocomposite contains amide, hydroxyl, and carboxyl groups. These functional groups are able to attract silver ions and provide an electron source for the Ag reduction process. Therefore, AgNPs were formed and uniformly distributed in SS polymer chains. This result agrees well with the SEM-EDS results (Figure 5). Typically, the synthesized NPs are likely to agglomerate. The in situ reduction of silver ions into AgNPs in SS matrix has been demonstrated as an effective method to obtain good distribution and dispersion of AgNPs in the SS polymer matrix, where SS in the system acts as a reducing and/or a stabilizing agent. Similar results were reported by Das et al. [30], Li et al. [31], and Chao et al. [32]. The surface morphology of the untreated and treated silk fabrics is presented in Figure 5a,b, respectively. An apparent difference between the untreated and treated silk fabrics was observed. The presence of AgNPs uniformly distributed on the treated fabrics is shown in Figure 5b, while no such particles were observed on the untreated fabrics (Figure 5a). Figure 5c,d shows the energy dispersive spectra and AgNP distribution of the fiber treated with SS-AgNP nanocomposites. It was confirmed that the silver element was present and uniformly distributed on the treated fiber. The Ag signals at 3 keV were observed. Other signals were due to elements in the SS matrix.

The crystalline structure of AgNPs in the nanocomposites was confirmed by XRD (Figure 6). Four peaks located at 2θ values of 14.06° , 17.22° , 20.75° , and 28.04° in both patterns corresponded to the crystalline diffraction of silk fibers [33,34]. After in situ synthesis of AgNPs, three more peaks appeared at 2θ values of 38.41° , 46.08° , and 64.45° , which agreed well with the (111), (200), and (220) diffractions of the face centered cubic (fcc) structure of metallic Ag [35]. Further investigation of the oxidation state of Ag in the nanocomposites was conducted by XPS. Figure 7 shows the XPS spectrum

of Ag (3d). Two main peaks can be seen in the Ag (3d) binding energy region, in which the binding energies of Ag (3d_{5/2}) and Ag (3d_{3/2}) are located at 368.18 and 374.18 eV, respectively. The two peak positions corresponded to the characteristics of metallic silver, confirming that the NPs observed on the treated silk fibers were Ag⁰ particles [36,37]. This verified that AgNPs were successfully loaded onto the silk fibers. The results suggested that AgNPs with excellent crystalline structure and uniform distribution were successfully synthesized on the SS functionalized silk fibers.

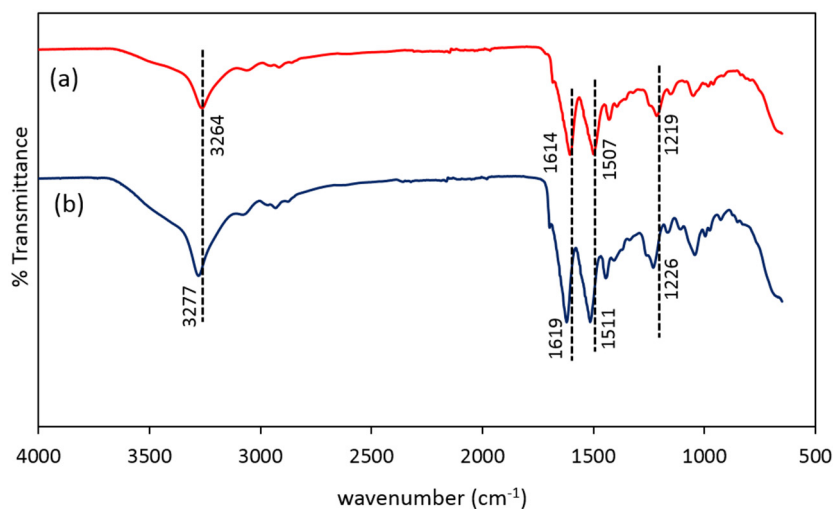


Figure 4. Fourier transform infrared spectroscopy (FTIR) spectra (a) original silk; and (b) SS-AgNP finished silk.

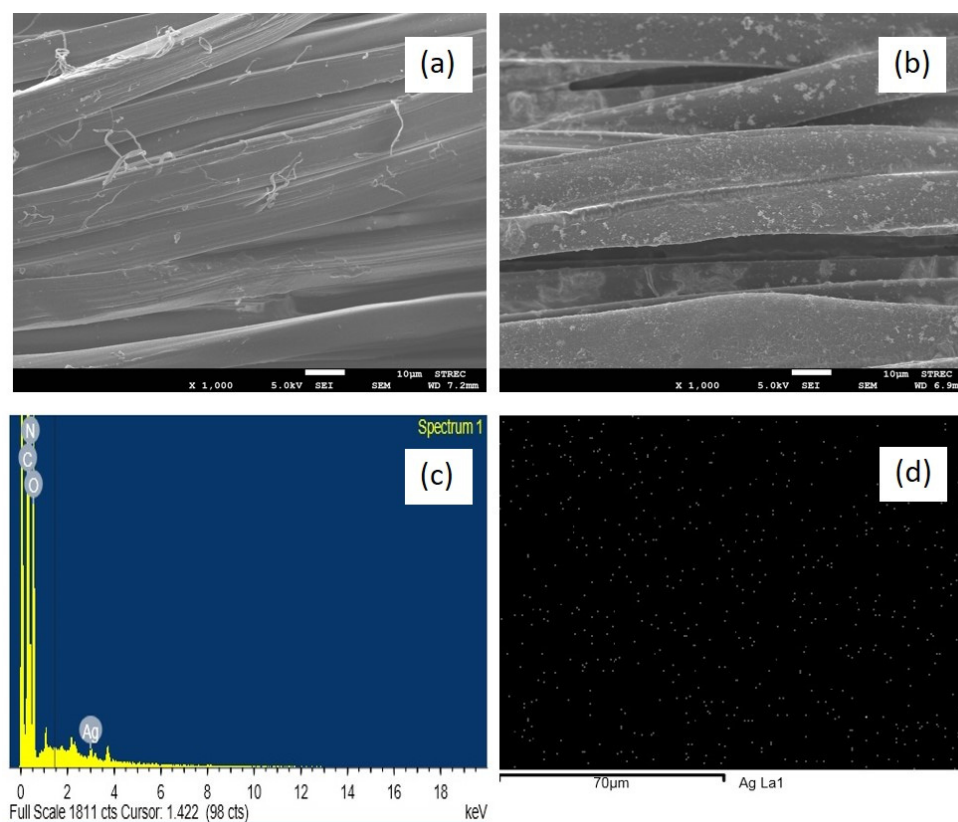


Figure 5. The Scanning Electron Microscope (SEM-EDX), images of SS-AgNP functionalized silk fabrics (a) untreated at 1000 \times ; (b) treated at 1000 \times ; (c,d) EDX pattern and AgNP distribution of treated fabrics.

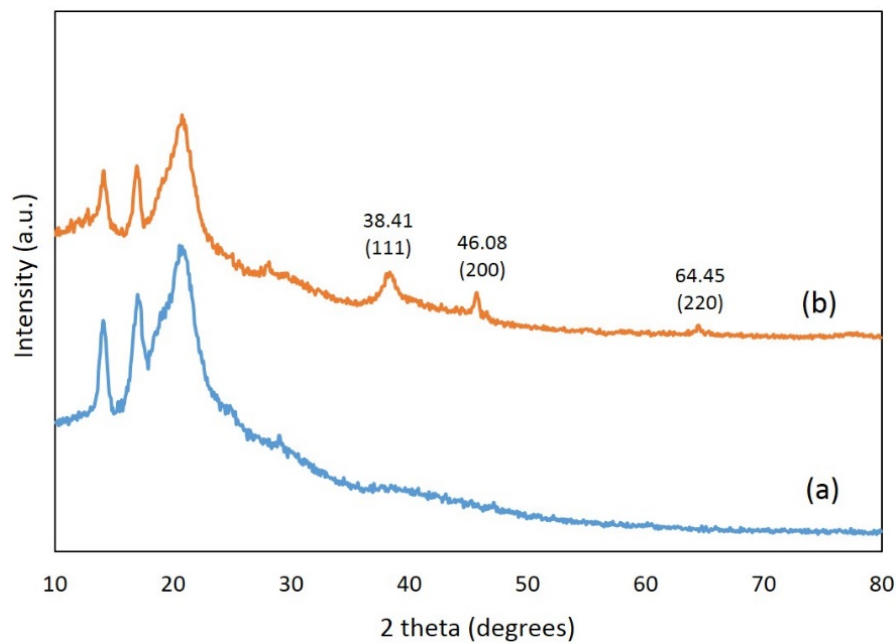


Figure 6. X-ray diffraction (XRD) spectra of (a) SS treated silk fabrics and (b) SS-AgNP treated silk fabrics.

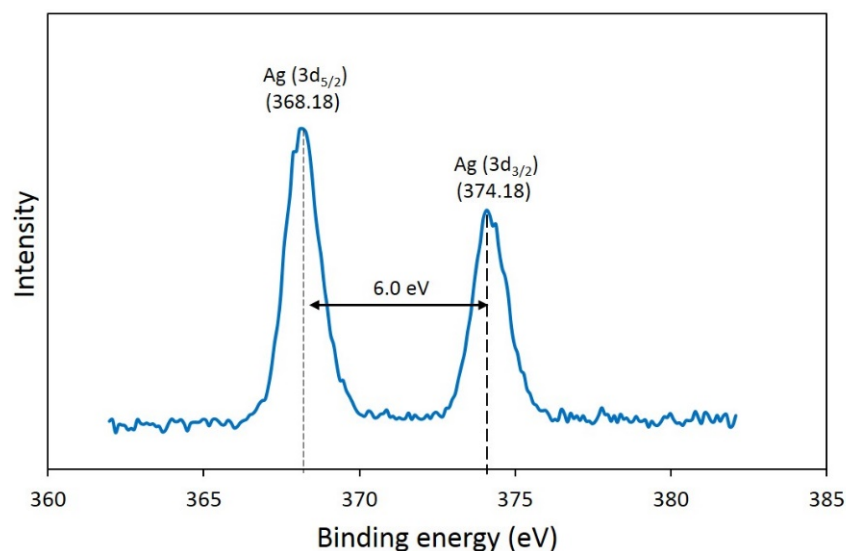
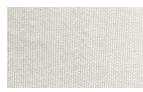



Figure 7. X-ray photoelectron spectroscopy (XPS) spectrum of SS-AgNP nanocomposites.

3.3. Color Coordinates

Table 4 shows the colorimetric coordinates of the untreated and SS-AgNP treated silk fabrics (using optimal condition from RSM). The treated fabric had a yellow color, suggesting the formation of AgNPs on the fabrics. Thus lightness (L^*), redness-greenness (a^*), yellowness-blueness (b^*) have changed due to the assembling of AgNPs on the fabric surface. The results indicated that the color of the treated samples was different from the untreated one. There was a noticeable decrease in L^* as the most significant change occurred on the color space due to the surface Plasmon resonance on the silver nanoparticle surfaces [21,29].

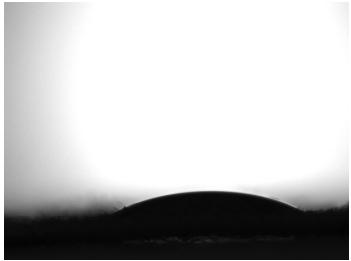
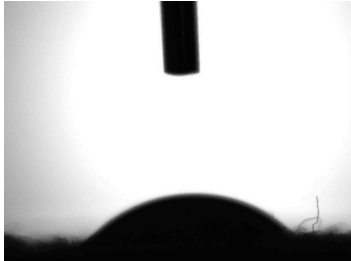
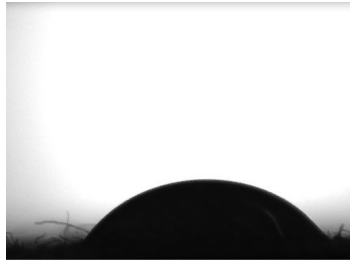
Table 4. Color coordinates of untreated and SS-AgNP treated silk fabric.

Samples	L^*	a^*	b^*	ΔE^*	Fabric Images
untreated	90.89	4.23	−7.36	–	
treated	69.24	5.78	−3.25	22.09	

3.4. Contact Angle

The water contact angle can indicate the hydrophobicity and wettability of textiles. The greater the contact angle is, the less hydrophilic is the textile surface. Large contact angle corresponds to low wettability, whereas small contact angle corresponds to high wettability. Table 5 shows the contact angles of the untreated, SS-treated, SS-AgNP treated silk fabrics. The results showed that the contact angle of untreated silk fabric was 12.28, indicating high hydrophilicity, which is a well-known characteristic of silk textiles. This can be attributed to the large number of polar groups (carboxyl, hydroxyl, and amino groups) on both the backbones and side chains of the polypeptide molecules presented in silk fibers [38]. The SS and SS-AgNP treated fabrics became less hydrophilic due to increasing contact angles. This can be attributed to the increase in roughness of the silk fabric surface [39].

Table 5. The water contact angles of untreated and treated silk fabrics.

Untreated Silk	SS-Treated Silk	SS-AgNP Treated Silk
		
$12.28^\circ \pm 3.7$	$35.15^\circ \pm 2.3$	$41.23^\circ \pm 3.8$

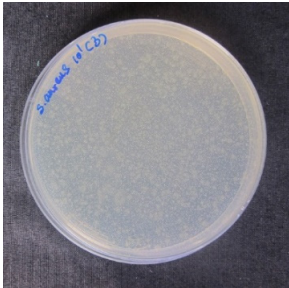

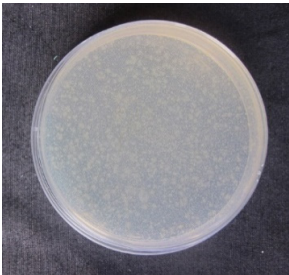

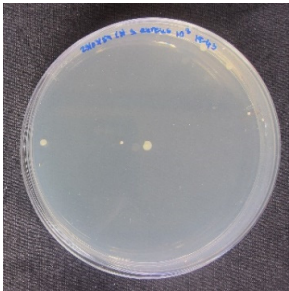
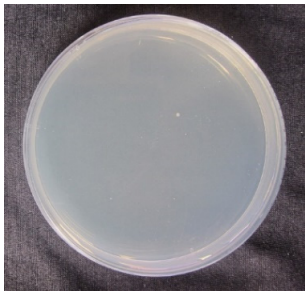
3.5. Evaluation of UV Protection Property

The protection against UV radiation provided by a material is determined by its UPF. The untreated silk fabrics used in this study had a low UPF of 5.14, significantly below the protection value of 15.0. This agrees well with the work of Becker et al. [40] who reported that fabrics made from SS depleted silk are prone to light-induced damage, against which a UV-absorber provides protection. Therefore, unless specially treated, standard silk fabrics do not provide sufficient skin protection against strong UV radiation [41]. After functionalization with SS-AgNP nanocomposites, the UPF values increased in line with the SS and AgNO₃ levels, as shown in Figure 2a. Most of the treated silk fabrics exhibited “excellent UV protection”, with UPF values greater than 40. The exception was samples whose SS contents were less than 10,000 ppm. These results also suggested that a uniform distribution of AgNPs improved UV protection. The protection is due to the absorption properties of AgNPs in the visible and UV ranges. The size of AgNPs generated in our work was in the range of 9–40 nm, which had a yellow color with a typical absorption peak at 420 nm. A similar size of AgNPs in the SS system was also reported by Aramwit et al. [21].

3.6. Antibacterial Activity of SS-AgNP Finished Silks

The untreated and SS-treated silk fabrics did not exhibit antibacterial effect against both *E. coli* and *S. aureus* (Table 6). The antibacterial activity of SS-AgNP treated fabrics increased with increasing AgNO_3 contents, hence amount of AgNPs. It has been reported that any AgNP composites exhibit their antimicrobial activity by the gradual release of Ag^+ . To evaluate the antibacterial efficiency, additional experiments were conducted using our RSM optimal condition. The time-dependent release of Ag^+ from the SS-AgNP treated silk fabrics was monitored in comparison to AgNP-treated silk fabrics as a positive control and they were fabricated by a UV-assisted method, in which the silk fabrics were soaked in a AgNO_3 aqueous solution and irradiated under UV light [42], as shown in Figure 8. At the initial stage (before 10 h), both AgNP-treated and SS-AgNP treated silk released similar concentration of Ag^+ . However, after 10 h the SS-AgNP treated silk exhibited higher Ag^+ concentrations than those of AgNP-treated ones at all times, indicating the higher Ag^+ release rate of the SS-AgNP treated samples. The higher concentrations of Ag^+ suggest stronger antimicrobial activity [43]. The Ag^+ release from AgNPs treated fabrics prepared by UV-assisted synthesis can last for 168 h. While, for SS-AgNP treated fabrics, the Ag^+ release can be extended to 312 h. It was apparent that the antimicrobial activity of SS-AgNP treated fabrics lasts longer than that of AgNPs treated ones. It is suggested that the presence of SS could prevent a direct exposure of AgNPs to oxygen, and hence slow down the release of Ag^+ . However, too excessive levels of SS affected the antibacterial activity in that antibacterial activity decreased when SS levels were greater than 11,000 ppm.

Table 6. Images of antibacterial activities against two bacterial types.

Samples	<i>S. aureus</i>	<i>E. coli</i>
Untreated silk		
SS treated silk		
SS-AgNP treated silk		

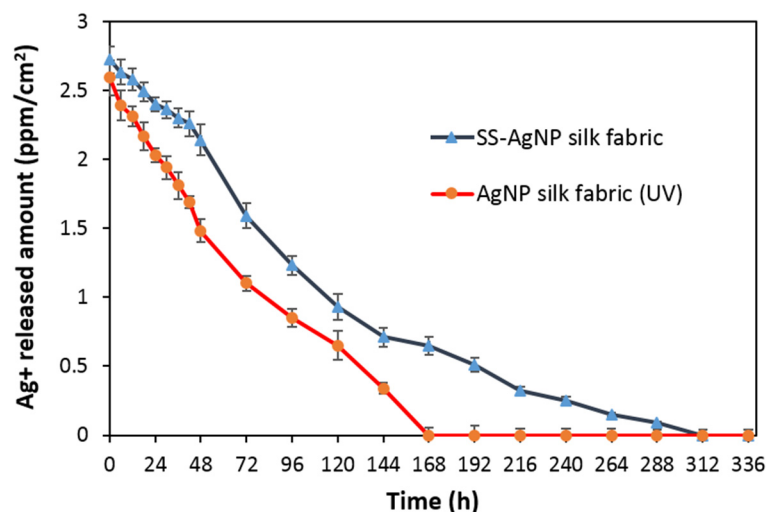


Figure 8. Ag⁺ release profile of SS-AgNP and AgNP finished silks.

3.7. Washing Fastness

To assess the durability, the SS-AgNP finished silk was prepared according to the optimal conditions obtained from the RSM model (AgNO₃ 1300 ppm, SS 9800 ppm) and washed for 10 and 20 cycles, as shown in SEM images (Figure 9). Before washing more SS-Ag nanocomposite on silk fibers was observed than on those after washing. Then, the evaluation of UV protection (UPF) and antibacterial activity against two key strains of bacterial cells were conducted and are presented in Table 7. The %reduction decreases with increasing washing cycles. However, it still shows high %reduction of 88.46 for *S. aureus* and 90.15 for *E. coli* after 20 washing cycles. The UV protection property slightly decreased after 20 washing cycles. It suggested the strong adhesion between SS and silk fibers. SS may not only provide reduction power in the fabrication of antibacterial silk materials, but also serve as an excellent 3-dimension matrix for the high-density loading of AgNPs.

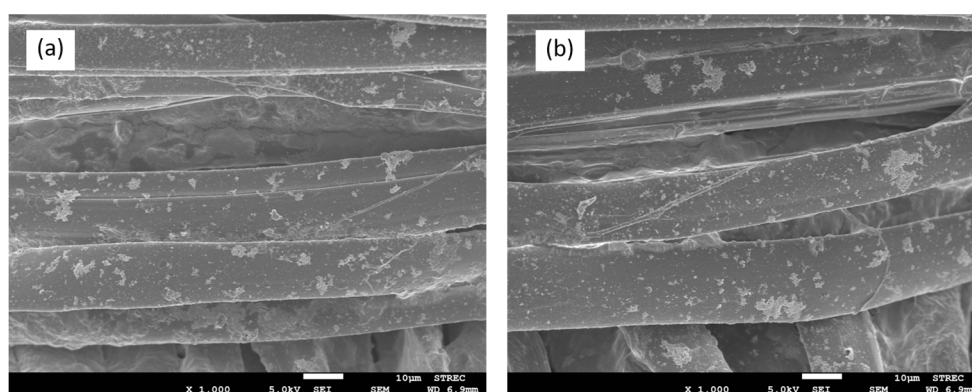


Figure 9. The SEM images of SS-AgNP finished silk fabrics (a) after 10 and (b) 20 washing cycles.

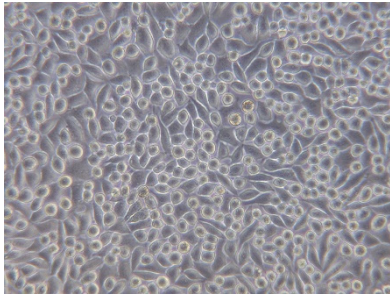
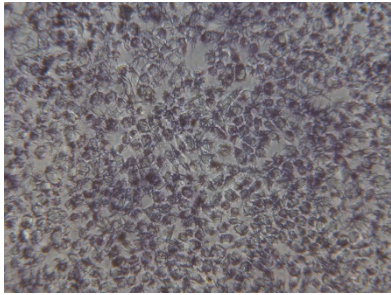
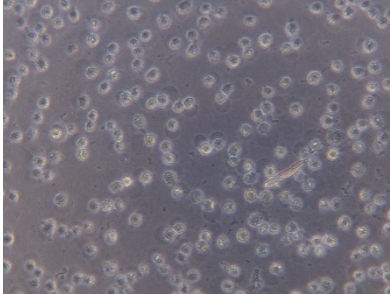
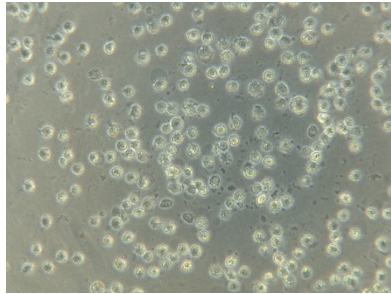
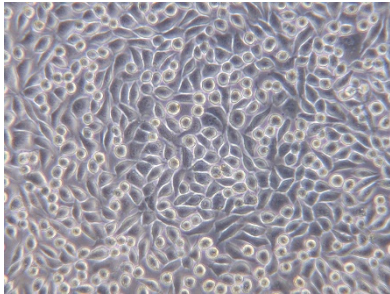
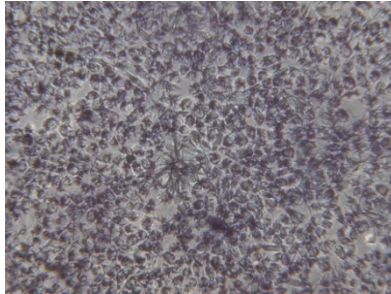
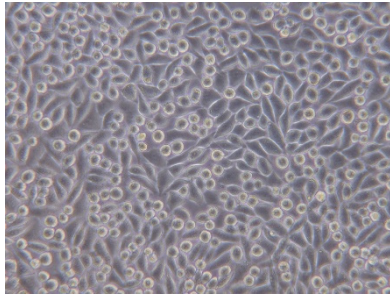
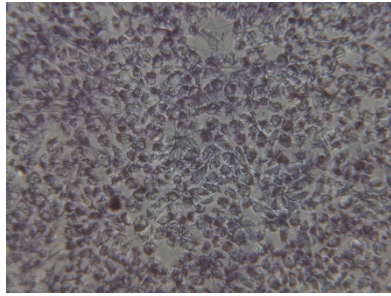
Table 7. Properties of UV protection and antibacterial activity of SS-AgNP samples after washing.

Samples	Washing Times	UPF	%reduction	
			<i>S. aureus</i>	<i>E. coli</i>
Untreated	–	5.1	–	–
Finished	0	42.8	99.3	100.0
	10	39.4	93.5	95.4
	20	35.6	88.5	90.2

3.8. Cytotoxicity Test

A cytotoxicity test is a method for testing materials and products that come into contact with people. In this study, cytotoxicity was investigated using the MTT cytotoxicity test (ISO 10993-5 [28]). A %cell viability greater than 70%, compared to a control, means the tested material is safe and non-toxic. Table 8 shows the cytotoxicity results of SS-AgNP treated silks. The %cell viability of untreated and treated silks were 95% and 79%, respectively, which were greater than 70, indicating non-toxicity to mammalian cells. Therefore, the obtained SS and AgNO₃ contents from the RSM model are considered to be safe and effective in their antibacterial activity against *E. coli* and *S. aureus*.

Table 8. Images of cytotoxicity testing of SS-AgNP finished silk.

No.	Sample	Before Dyed ($\times 200$)	After Dyed ($\times 200$)
1	Negative control		
2	Positive control		
3	Untreated silk		
4	Treated silk		

4. Conclusions

An environmental-friendly, economical, and simple one pot formulation for enhanced UV protection and antibacterial properties finished on silk fabrics was developed and optimized. SS can be considered a very promising material for silk surface functionalization via the in situ reduction of silver salts. Because it has several advantages: (1) SS could absorb Ag ions and further reduce them to AgNPs without any other substances; (2) SS contained strong polar functional groups, which could coordinate Ag ions and stabilize AgNPs; (3) SS served as a 3-dimensional matrix for high-density loading of AgNPs; and (4) the presence of SS could prevent direct exposure of AgNPs to oxygen, and hence slow down the release of silver ions. The optimal formulation identified by RSM exhibited excellent UV protection and antibacterial activities against *E. coli* and *S. aureus*, non-toxicity to mammalian cells, as well as laundering durability after 20 washing cycles.

Supplementary Materials: The following are available online at www.mdpi.com/2079-6412/7/9/145/s1, Figure S1: Predicted vs experimental values for (a) UPF, (b) %reduction of *E. coli*, and (c) %reduction of *S. aureus*.

Acknowledgments: The authors gratefully acknowledge the financial support provided by the Faculty of Science and Technology, Thammasat University (Contract No. 19/2559). Moreover, the authors acknowledge the Central Scientific Instrument Center (CSIC) for supporting the characterization of the finished fabrics.

Author Contributions: Pisutsaran Chitichotpanya proposed the research topic. Pisutsaran Chitichotpanya and Chayanisa Chitichotpanya conceived and designed the experiments. Pisutsaran Chitichotpanya performed the experiments and carried out the testing. Pisutsaran Chitichotpanya wrote the paper and Chayanisa Chitichotpanya edited it.

Conflicts of Interest: The authors report no conflicts of interest.

References

1. Van der Rhee, H.J.; De Vries, E.; Coebergh, J.W. Regular sun exposure benefits health. *Med. Hypotheses* **2016**, *97*, 34–37. [[CrossRef](#)] [[PubMed](#)]
2. Yu, Y.; Hurren, C.; Millington, K.R.; Sun, L.; Wang, X. Understanding the influence of fibre, yarn and fabric parameters on UV protection of wool-knitted fabrics. *J. Text. Inst.* **2017**, *108*, 1609–1617. [[CrossRef](#)]
3. Lu, H.; Fei, B.; Xin, J.H.; Wang, R.; Li, L. Fabrication of UV blocking nanohybrid coating via miniemulsion polymerisation. *J. Colloid Interface Sci.* **2006**, *300*, 111–116. [[CrossRef](#)] [[PubMed](#)]
4. Gowri, S.; Almeida, L.; Amorim, T.; Carneiro, N.; Souto, A.P.; Esteves, M.F. Polymer nanocomposites for multifunctional finishing of textiles—A review. *Text. Res. J.* **2010**, *80*, 1290–1306. [[CrossRef](#)]
5. Nussbaumer, R.J.; Caseri, R.; Smith, P.; Tervoort, T.A. Pol-ymer TiO₂ nanocomposites: A route towards visually trans-parent broadband UV filters and high refractive index materials. *Macromol. Mater. Eng.* **2003**, *288*, 44–49. [[CrossRef](#)]
6. Pisitsak, P.; Hutakamol, J.; Jeenapak, S.; Wanmanee, P.; Nuammaiphum, J.; Thongcharoen, R. Natural dyeing of cotton with xylocarpus granatum bark extract: Dyeing, fastness, and ultraviolet protection properties. *Fibers Polym.* **2016**, *17*, 560–568. [[CrossRef](#)]
7. Mongkholrattanasit, R.; Punrattanasin, N.; Rungruangkitkrai, N.; Somboon, B.; Narumol, N.; Nakpathom, M. Dyeing, fastness and UV protection properties of cotton fabric dyed with mangrove bark extract. *Cell. Chem. Technol.* **2016**, *50*, 163–171.
8. Cho, K.Y.; Moon, J.Y.; Lee, Y.W.; Lee, K.G.; Yeo, J.H.; Kweon, H.Y.; Kim, K.H.; Cho, C.S. Preparation of self-assembled silk sericin nanoparticles. *Int. J. Biol. Macromol.* **2003**, *32*, 36–42. [[CrossRef](#)]
9. Doakhan, S.; Montazer, M.; Rashidi, A.; Moniri, R.; Moghadam, M.B. Influence of sericin/TiO₂ nanocomposite on cotton fabric: Part 1. Enhanced antibacterial effect. *Carbohydr. Polym.* **2013**, *94*, 737–748. [[CrossRef](#)] [[PubMed](#)]
10. Aramwit, P.; Damrongsakkul, S.; Kanokpanont, S.; Srichana, T. Properties and anti-tyrosinase activity of sericin from various extraction methods. *Biotechnol. Appl. Biochem.* **2010**, *55*, 91–98. [[CrossRef](#)] [[PubMed](#)]
11. Mondal, M.; Trivedy, K.; Kumar, S.N. The silk proteins, sericin and fibroin in silkworm, *Bombyx mori* Linn.—A review. *Casp. J. Environ. Sci.* **2007**, *5*, 63–76.

12. Zhaorigetu, S.; Yanaka, N.; Sasaki, M.; Watanabe, H.; Kato, N. Inhibitory effects of silk protein, sericin on UVB-induced acute damage and tumor promotion by reducing oxidative stress in the skin of hairless mouse. *J. Photochem. Photobiol. B* **2003**, *71*, 11–17. [[CrossRef](#)]
13. Zhang, Y.Q. Applications of natural silk protein sericin in biomaterials. *Biotechnol. Adv.* **2002**, *20*, 91–100. [[CrossRef](#)]
14. Kundu, S.C.; Dash, B.C.; Dash, R.; Kaplan, D.L. Natural protective glue proteins, sericin bioengineered by silkworms: Potential for biomedical and biotechnological applications. *Prog. Polym. Sci.* **2008**, *33*, 998–1012. [[CrossRef](#)]
15. Fabiani, C.; Pizzichini, M.; Spadoni, M.; Zeddit, G. Treatment of waste water from silk degumming processes for protein recovery and water reuse. *Desalination* **1996**, *105*, 1–9. [[CrossRef](#)]
16. Drader, M.; Aranda, P.; Ruiz-Hitzky, E. Bionanocomposites: A new concept of ecological, bioinspired, and functional hybrid materials. *Adv. Mater.* **2007**, *19*, 1309–1319. [[CrossRef](#)]
17. Mangiacapra, P.; Gorrasi, G.; Sorrentino, A.; Vittoria, V. Biodegradable nanocomposites obtained by ball milling of pectin and montmorillonites. *Carbohydr. Polym.* **2006**, *64*, 516–523. [[CrossRef](#)]
18. Liu, S.; He, J.; Xue, J.; Ding, W. Efficient fabrication of transparent antimicrobial poly(vinyl alcohol) thin film. *J. Nanopart. Res.* **2009**, *11*, 553–560. [[CrossRef](#)]
19. Wattanodorn, Y.; Jenkana, R.; Atorngitjawatd, P.; Wirasate, S. Antibacterial anionic waterborne polyurethanes/Ag nanocomposites with enhanced mechanical properties. *Polym. Test.* **2014**, *40*, 163–169. [[CrossRef](#)]
20. Lu, Z.; Xiao, J.; Wang, Y.; Meng, M. In Situ synthesis of silver nanoparticles uniformly distributed on polydopamine-coated silk fibers for antibacterial application. *J. Colloid Interface Sci.* **2015**, *452*, 8–14. [[CrossRef](#)] [[PubMed](#)]
21. Aramwit, P.; Bang, N.; Ratanavaraporn, J.; Ekgasit, S. Green synthesis of silk sericin-capped silver nanoparticles and their potent anti-bacterial activity. *Nanoscale Res. Lett.* **2014**, *9*, 79. [[CrossRef](#)] [[PubMed](#)]
22. Selvakannan, P.R.; Swami, A.; Srisathiyarayanan, D.; Shirude, P.S.; Pasricha, R.; Mandale, A.B.; Sastry, M. Synthesis of aqueous Au core–Ag shell nanoparticles using tyrosine as a pH-dependent reducing agent and assembling phase-transferred silver nanoparticles at the air–water interface. *Langmuir* **2004**, *20*, 7825–7836. [[CrossRef](#)] [[PubMed](#)]
23. Aramwit, P.; Kanokpanont, S.; Nakpheng, T.; Srichana, T. The effect of sericin from various extraction methods on cell viability and collagen production. *Int. J. Mol. Sci.* **2010**, *11*, 2200–2211. [[CrossRef](#)] [[PubMed](#)]
24. Box, G.E.P.; Wilson, K.B. On the experimental attainment of optimum conditions. *J. R. Stat. Soc. Ser. B* **1951**, *13*, 1–45.
25. *AS/NZS 4399:1966 Standard Test Method for Sun Protective Clothing Evaluation and Classification*; Standards Australian: Homebush, Australia; Standards New Zealand: Wellington, New Zealand, 1996.
26. *AATCC 100-1999 Standard Test Method for Assessment of Antibacterial Finishes on Textile Materials*; American Association of Textile Chemists and Colorists technical manual; American Association of Textile Chemists and Colorists (AATCC): Research Triangle Park, NC, USA, 1999.
27. *AATCC 61-1996 Standard Test Method for Color Fastness to Laundering, Home and Commercial: Accelerated*; American Association of Textile Chemists and Colorists (AATCC): Research Triangle Park, NC, USA, 1996.
28. *ISO 10993-5 Standard Test Method for Biological Evaluation of Medical Devices—Part 5: Tests for In Vitro Cytotoxicity*; International Organization for Standardization (ISO): Geneva, Switzerland, 2009.
29. Zhang, G.; Liu, Y.; Gao, X.; Chen, Y. Synthesis of silver nanoparticles and antibacterial property of silk fabrics treated by silver nanoparticles. *Nanoscale Res. Lett.* **2014**, *9*, 216–224. [[CrossRef](#)] [[PubMed](#)]
30. Das, R.; Gang, S.; Nath, S.S. Preparation and antibacterial activity of silver nanoparticles. *J. Biomater. Nanobiotechnol.* **2011**, *2*, 472–475. [[CrossRef](#)]
31. Li, W.R.; Xie, X.B.; Shi, Q.S.; Zeng, H.Y.; Ou-Yang, Y.S.; Chen, Y.B. Antibacterial activity and mechanism of silver nanoparticles on *Escherichia coli*. *Appl. Microbiol. Biotechnol.* **2010**, *85*, 1115–1122. [[CrossRef](#)] [[PubMed](#)]
32. Chao, L.; Xiansong, W.; Feng, C.; Chunlei, Z.; Xiao, Z.; Kan, W.; Xiangcui, D. The antifungal activity of graphene oxide–silver nanocomposites. *Biomaterials* **2013**, *34*, 3882–3890.
33. Andiappan, M.; Kumari, T.; Sundaramoorthy, S.; Meiyazhagan, G.; Manoharan, P.; Venkataraman, G. Comparison of eri and tasar silk fibroin scaffolds for biomedical applications. *Prog. Biomater.* **2016**, *5*, 81–91. [[CrossRef](#)] [[PubMed](#)]

34. Lu, Q.; Hu, X.; Wang, X.; Kluge, J.A.; Lu, S.; Cebe, P.; Kaplan, D.L. Water-insoluble silk films with silk I structure. *Acta Biomater.* **2010**, *6*, 1380–1387. [[CrossRef](#)] [[PubMed](#)]
35. Qu, R.; Gao, J.; Tang, B.; Ma, Q.; Qu, B.; Sun, C. Preparation and property of polyurethane/nanosilver complex fibers. *Appl. Surf. Sci.* **2014**, *294*, 81–88. [[CrossRef](#)]
36. Kaspar, T.C.; Drouday, T.; Chambers, S.A.; Bagus, P.S. Spectroscopic evidence for Ag (III) in highly oxidized silver films by X-ray photoelectron spectroscopy. *J. Phys. Chem. C* **2010**, *114*, 21562–21571. [[CrossRef](#)]
37. Yue, X.; Lin, H.; Yan, T.; Zhang, D.; Lin, H.; Chen, Y. Synthesis of silver nanoparticles with sericin and functional finishing to cotton fabrics. *Fibers Polym.* **2014**, *15*, 716–722. [[CrossRef](#)]
38. Kan, C.; Lam, Y. The effect of plasma treatment on water absorption properties of silk fabrics. *Fibers Polym.* **2015**, *16*, 1705–1714. [[CrossRef](#)]
39. Chen, F.; Liu, X.; Yang, H.; Dong, B.; Zhou, Y.; Chen, D.; Hu, H.; Xiao, X.; Fan, D.; Zhang, C. A simple one-step approach to fabrication of highly hydrophobic silk fabrics. *Appl. Surf. Sci.* **2016**, *360*, 207–212. [[CrossRef](#)]
40. Becker, M.A.; Willman, P.; Tuross, N.C. The US first ladies gowns: A biochemical study of silk preservation. *J. Am. Inst. Conserv.* **1995**, *34*, 141–152. [[CrossRef](#)]
41. Reinert, G.; Fuso, F.; Hilfiker, R.; Schmidt, E. UV-protecting properties of textile fabrics and their improvement. *Text. Chem. Color.* **1997**, *29*, 36–43.
42. Lu, Z.S.; Meng, M.; Jiang, Y.; Xie, J. UV-assisted in situ synthesis of silver nanoparticles on silk fibers for antibacterial applications. *Colloids Surf. A* **2014**, *447*, 1–7. [[CrossRef](#)]
43. Brett, D.W. A discussion of silver as an antimicrobial agent: Alleviating the confusion. *Ostomy/Wound Manag.* **2006**, *52*, 34–41.



© 2017 by the authors. Licensee MDPI, Basel, Switzerland. This article is an open access article distributed under the terms and conditions of the Creative Commons Attribution (CC BY) license (<http://creativecommons.org/licenses/by/4.0/>).